Hydrodynamics of Electrofluidization: Separation of Pyrites from Coal

Dry, electrostatic separation is a potentially efficient method of removing pyrites from coal. However, progress in the past was hampered by a lack of a quantitative analysis of the process. To help us design better separation equipment, we have developed a hydrodynamic model of separation of pyrites from coal in a batch electrofluidized bed. The simulations were done on a Cray-2 computer. The input variables include the surface charge of the particles and the solids stress, which were measured.

Realistic shapes and sizes of bubbles were computed with and without an applied electric field for a two-dimensional bed with a central jet. The bubble sizes and the rising velocities were smaller with an applied field, consistent with observations. Computed electrophoretic mobilities in the fluidized bed will be useful for a better design of continuous beds.

Y. T. Shih, Dimitri Gidaspow and Darsh Wasan
Department of Chemical Engineering
Illinois Institute of Technology
Chicago, IL 60616

Introduction

The overall objective of our investigation is to develop improved dry electrostatic separation methods of removing sulfur-bearing compounds from Illinois coal. When coal is pulverized for combustion, iron pyrites occur as distinct particles that can be removed by the application of an electric field (Inculet et al., 1982; Gidaspow et al. 1986a). Separation is possible because the iron particles acquire a charge different from the rest of coal. This surface charge can be acquired triboelectrically, by induction or by corona discharge. Until recently, electrostatic methods used in the past (Ralston, 1961; Moore, 1973; Abel et al., 1973) involved expensive rotor-type machines that involved scraping of the solids that stuck to the electrodes. This problem has recently been solved (Gidaspow et al. 1986a) by the use of perforated electrodes through which cleaned coal and pyrite-enriched coal are continuously removed from a fluidized bed fed with a stream containing coal and pyrites. To achieve an optimum separation, a mathematical model of the process is needed. *That is the specific objective of this paper.* A hydrodynamic model of electrofluidization was developed. The model is an extension of the single-particle-size hydrodynamic model reviewed by Gidaspow (1986) and of the binary size hydrodynamic model of fluidization of Gidaspow et al. (1986b). It is based on the early work of Jackson (1963), Soo (1967), and others as reviewed by Gidaspow (1986). The differential equations used are similar to those of Rosensweig et al. (1983) for a single size fluidized bed with a magnetic field. Simulations were done for a batch electrofluidized bed using the University of Minnesota Cray-2 computer. The computed bubbles with and without an applied electric field were compared to experiments, when available.

The earliest reported studies of electrofluidized bed mechanisms are those by Katz (1967) and Katz and Sears (1969), who noted that electrofluidized beds can be stabilized by the presence of corona currents. Johnson and Melcher (1975) presented a heuristic description of electrofluidized bed dynamics without the complications of corona discharge. Pictures were shown to demonstrate the dramatic changes in bubble shape that can be caused by the application of an electric field. Colver (1979) also indicated that bubbles can be controlled in size and intensity by the application of suitably applied electric fields. Zahedi and Melcher (1976) used electrofluidization in the filtration of submicron aerosols. The importance of the interparticle forces in an electrofluidized bed was later discussed by Dietz and Melcher (1978). Colver (1979) gave a general review of the subject. More recently, some of the effects of electric field on the fluidized systems, such as the elimination and deformation of bubbles and the expansion of the bed were investigated by Ademoyega (1981).

A Hydrodynamic Model

Hydrodynamic models of fluidization use the principles of conservation of mass and momentum for each phase. Gidaspow

Correspondence concerning this paper should be addressed to Dimitri Gidaspow.

(1986) has given a detailed review of the hydrodynamic modeling of fluidization. The model developed here for electrofluidization is essentially an extension of the K-FIX algorithm (Rivard and Torrey, 1977). The K-FIX computer code is written in a modular form and has been demonstrated to be adaptable to a variety of multiphase flow problems (Ettehadieh, 1982; Syamlal, (1985). Syamlal 1985 and Gidaspow et al. (1985) present a manual for an extension of the K-FIX algorithm to three phases.

Governing equations

The electrofluidization system considered in this study consists of a gas and two distinct particular phases. The two types of particles, coal and pyrite, contain different surface charges and differ in both density and diameter. The model, however, can be easily extended to include N particular phases. The set of conservation equations for electrofluidization is given below. Note that the subscript 1 is used to indicate the gas phase.

Continuity Equations

$$\frac{\partial}{\partial t}(\rho_k \epsilon_k) + \nabla \cdot (\epsilon_k \rho_k v_k) = 0 \tag{1}$$

Momentum Equations

$$\frac{\partial}{\partial t}(\rho_k \epsilon_k v_k) + \nabla \cdot (\epsilon_k \rho_k v_k v_k) = -\epsilon_k \nabla P + \rho_k \epsilon_k g + G_k \nabla \epsilon_1 + \sum_{l=1}^{N} K_{kl}(v_l - v_k) + q_k E \tag{2}$$

where

$$\sum_{k=1}^{N} \epsilon_k = 1 \tag{3}$$

The gas phase is considered to be ideal and the particulate phases, coal and pyrite, are considered to have constant densities.

Equation of State

$$\rho_1 = \frac{P}{RT}$$

$$\rho_k = \rho_{sk} \quad \text{for } k \geq 2 \tag{4}$$

Drag law: gas-particle interaction

In Gidaspow's (1986) review of hydrodynamic modelings of fluidization, gas-particle correlation was derived from the Ergun equation and the generalized single-sphere drag law. It is generalized as follows for each particular phase in a multiparticulate system, as done by Gidaspow et al. (1986b).

$$K_{1k} = K_{k1} = \frac{150(1-\epsilon_1)\epsilon_k \mu_1}{\epsilon_1 (d_k \phi_k)^2} + \frac{1.75 \rho_1 |v_1 - v_k| \epsilon_k}{(d_k \phi_k)} \qquad 0.2 \leq \epsilon_1 < 0.8$$

$$= \frac{3}{4} C_{Dk} \frac{\epsilon_1 |v_1 - v_k| \rho_1 \epsilon_k}{(d_k \phi_k)} f(\epsilon_1) \qquad 0.8 \leq \epsilon_1 \leq 1.0 \tag{5}$$

where

$$f(\epsilon_1) = \epsilon_1^{-2.65} \tag{6}$$

$$C_{DK} = \frac{24}{Re_k}(1 + 0.15 Re_k^{0.687}) \qquad Re_k < 1{,}000$$

$$= 0.44 \qquad Re_k \geq 1{,}000 \tag{7}$$

and

$$Re_k = \frac{d_k |v_1 - v_k| \rho_1 \epsilon_1}{\mu_1} \tag{8}$$

The above relations were generalized in such a way that the momentum equations correctly add up to the mixture momentum equation, and that they agree with the usual principles of formulation of constitutive equations and observations to be discussed in a later section of this paper.

Particle-particle interactions

Collisions between particles with different velocities result in particle-particle friction. These interactions must be included in the governing equations to represent the momentum exchange between the particulate phases. An equation for such an interaction in a dilute mixture was first suggested by Soo (1967). Nakamura and Capes (1976) later derived a similar expression based on the conservation of linear momentum. They considered that the relative velocity after collision is equal to the relative velocity before collision times the usual coefficient of restitution. Such a correlation was used by Arastoopour et al. (1980) in a study of segregation of particles of different sizes in a pneumatic conveyor. Arastoopour et al. (1982) experimentally verified such an interaction in a pneumatic conveyor. Based on the Bagnold (1954) and Fedors and Landel (1979) studies, Syamlal (1985) and Gidaspow et al. (1986b) derived a similar expression for particle-particle interactions for dense phases. Their formula, however, requires an estimate of maximum packings of each phase. In view of this, the Nakamura and Capes (1976) expression was adopted in this study due to its simplicity.

$$K_{\substack{k\ell \\ k,\ell \neq 1}} = \frac{3}{2}\alpha(1+e)\frac{\rho_k \rho_1 \epsilon_k \epsilon_1 (d_k + d_1)^2}{\rho_k d_k^3 + \rho_1 d_1^3} |v_k - v_1| \tag{9}$$

The collisions between the particles are plastic when the restitution coefficient $e = 0$; the collisions are elastic when $e = 1$. The value of α accounts for nonhead-on collisions. In countercurrent flow Gwyn (1986) calls such collisions the bang-bang type.

Solids stress

In a general formulation the solid momentum equations would contain solids stress terms that are a function of porosity, pressure, and the displacement tensors of solids velocities, gas velocity, and relative velocities. Such a general formulation with proper values of material constants does not exist today (Gidaspow, 1986). Only a normal component of the solids stress is considered in this study to prevent the particles from reaching impossibly low values of void fraction. As discussed in Gidaspow and Ettehadieh (1983a), such a term is also necessary to make the characteristics real and thereby to make the problem well

posed as an initial value problem. Rietma and Musters (1973) also introduced such a term into modeling of fluidization and have made measurements of this elasticity modulus in an inclined fluidized bed. Their latest report is in Piepers et al. (1984).

Recently, Gidaspow and Syamlal (1985) proposed a method to measure the stress modulus G using critical flow theory. They analyzed various hydrodynamic models for one-dimensional solid-gas flow and concluded that in a vacuum the critical flow velocity is

$$V_{s,\text{crit}} = \left(\frac{-G}{\rho_s}\right)^{1/2} \tag{10}$$

This critical velocity was measured in a specially designed bin (Gidaspow et al., 1985). The results give us G. For a mixture of 50 wt. % iron pyrites (150 μm), the measured modulus of elasticity was as follows.

$$G(\epsilon_1) = -10^{-8.76\epsilon_1 + 7.8} \quad \text{N/m}^2 \tag{11}$$

These values of G are about 80 times greater than those determined by Rietma and Musters (1973) for their particles. Equation 11 was used in the numerical computations. The values of G_k in Eq. 2 become:

$$\begin{aligned} G_k &= 0 \quad \text{for } k = 1 \\ &= \epsilon_k G(\epsilon_1) \quad \text{for } k = 2, \ldots, N \end{aligned} \tag{12}$$

Surface charge of particles

To model the electrofluidized bed, we need to know the surface charges of particles. The electric force acting on a particle in an electrostatic field is the product of its charge and the strength of the electric field applied, i.e., $q_k E$. Inculet et al. (1982) have indicated that the charging of the particles in a fluidized bed may take place by triboelectrification.

A pneumatic conveyor was designed and constructed to conduct a direct measurement of such a charge. The average surface charge per particle was measured by inserting a metallic ball probe through the sides of an electrostatic pneumatic conveyor. The probe, which is inserted in the stream of charged particles, will pick up a current that is proportional to the charge of the particles. Details of the experimental measurements were reported by Gidaspow et al. (1986a). The average surface charges of coal and pyrite particles obtained at various dew point temperatures and mass flow rates are shown in Figures 1 and 2. Both coal and pyrite particles carry negative charges. The average size of the particles used in the experiments was 212 μm. Experimental work is continuing. Although such surface charges of particles may be a function of particle velocity, a constant surface charge of particles was used in the calculations. The values used were:

$$q_{\text{pyrite}} = 10^{-12} \quad \text{Coulomb/particle} \tag{13}$$

$$q_{\text{coal}} = 10^{-13} \quad \text{Coulomb/particle} \tag{14}$$

These surface charges have been corrected to the appropriate sizes of particles used in the computations. A dew point temperature of 440F was chosen.

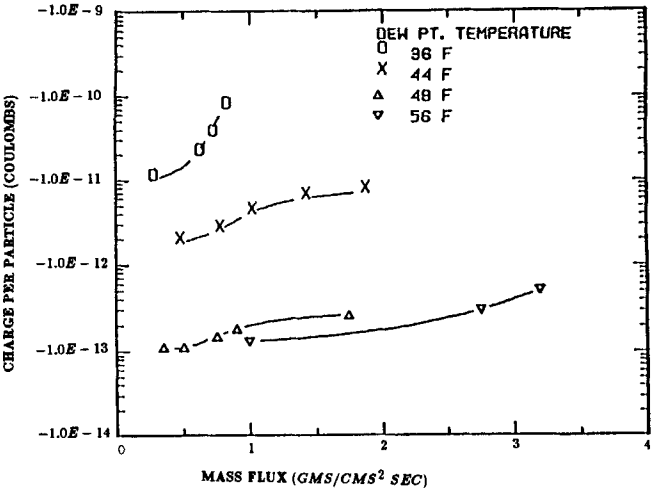

Figure 1. Surface charges of pyrites and coal.

It is interesting to compare the electrical force with the gravitational force acting on a pyrite particle in a free-fall electrostatic separator. The electrical force acting on a sphere of radius $a_p = 150$ μm with a uniform surface charge q_{pyrite} is $F_e = q_{\text{pyrite}} E$. The gravitational force is $F_g = (4/3)\pi a_p^3 \rho g$. At an electrical field strength of $E = 500$ V/cm and for the pyrite surface charge used, the ratio F_e/F_g is about 6.3%.

Case of negligible acceleration

The model can be better appreciated by considering a simplified situation. The momentum equations, Eqs. 2, in the vertical (y) direction with negligible acceleration and normal stress are as follows:

Gas Phase

$$0 = -\epsilon_1 \frac{dp}{dy} - \sum_{\ell=1}^{N} K_{1\ell}(v_1 - v_\ell) - \rho_1 \epsilon_1 g \tag{15}$$

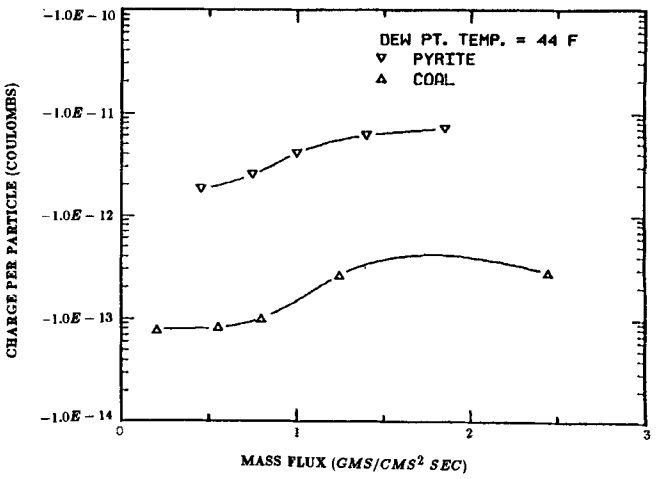

Figure 2. Surface charge of pyrites as a function of humidity.

Solid Phases

$$0 = -\epsilon_k \frac{dp}{dy} - \sum_{\ell=1}^{N} K_{k\ell}(v_k - v_\ell) - \rho_k \epsilon_k g \, \mathrm{L} \, q_k E \quad (16)$$

where g and E are the vertical components of vectors g and E in Eq. 2.

The sum of the above equations gives the mixture momentum equation:

$$-\frac{dp}{dy} = \sum_{k=1}^{N} \rho_k \epsilon_k g + \sum_{k=2}^{N} q_k E \quad (17)$$

pressure drop = weight of bed + electrical force

With no applied electric force, this equation is usually called the manometer formula, a well-known formula in Kunii and Levenspiel's (1969) book. Elimination of pressure in Eqs. 15 and 16 gives:

$$\frac{1}{\epsilon_1} \sum_{\ell=2}^{N} K_{1\ell}(v_1 - v_\ell) = \sum_{k=2}^{N} \epsilon_k(\rho_k - \rho_1)g + \sum_{k=2}^{N} q_k E \quad (18)$$

friction loss = buoyant force + electrical force

Equation 18 allows the determination of minimum fluidization velocity, U_{mf}, for electrofluidization of multisized particles. With zero solid velocities, we have

$$\frac{1}{\epsilon_1^2} \sum_{\ell=2}^{N} K_{1\ell} U_{mf} = \sum_{k=2}^{N} \epsilon_k(\rho_k - \rho_1)g + \sum_{k=2}^{N} q_k E \quad (19)$$

Dietz and Melcher (1978) reported that the overshoot pressure drop in an electrofluidized bed, actual pressure drop minus the pressure drop at zero electric field, increases almost linearly with an increase in voltage. Our Eq. 17 explains this phenomenon and provides an alternate scheme to measure the surface charge of particles. The slope of the plot for overshoot pressure drop vs. the electric field strength is the surface charge of the particles, q_K.

The "support" experiments of Dietz and Melcher also showed that the air velocity required to support a bed against an upper screen decreases as the applied voltage increases. This is because the electrofluidized bed is stabilized by the presence of an electric field. Ademoyega's (1981) experiments also confirmed these observations. The stabilized bed required higher gas velocities to fluidize it. Minimum fluidization velocity is higher when the applied voltage is higher. Our Eq. 19 clearly indicates that when E is higher, U_{mf} is higher.

We further note that for a multisize particle system there is no well-defined U_{mf} (Yang and Keairns, 1982). Rowe and Nienow (1975) and Chiba et al. (1979) discussed the difficulty of maintaining uniformity of the mixture and reproducibility of the experimental results. Syamlal (1985) compared the minimum fluidization velocity predicted by Eq. 19 at no external electric field with Rowe and Nienow's experiments. The variations were less than 30%.

Numerical scheme

The full governing equations, eqs. 1 and 2, along with the constitutive equations are solved for v_k, ϵ_k, and P using the ICE method (Rivard and Torrey, 1977; Ettehadieh, 1982; Syamlal, 1985; Gidaspow et al. 1985) with appropriate initial and boundary conditions. The computations are carried out using a mesh of finite-difference cells fixed in a two-dimensional space (Eulerian mesh). A tyical computational cell is shown in Figure 3. The scalar variables are located at the cell center and the vector variables at the cell boundaries.

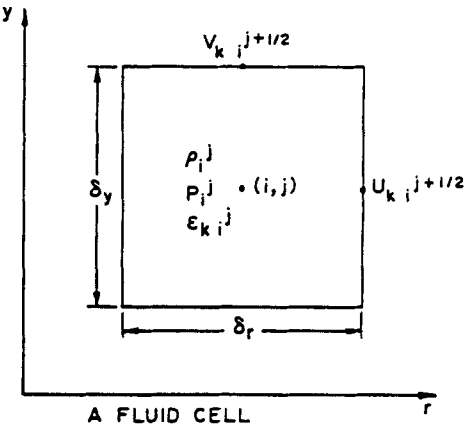

Figure 3. Computational cell.

The continuity equation is fully differenced implicitly, and the flux terms in continuity and momentum equations are full donor-cell differenced. The donor cell differencing helps to prevent a cell from getting drained completely, giving negative volume fractions, and also aids computational stability. The momentum equations are differenced over a staggered mesh of computational cells, Figure 4. Syamlal (1985) has given the detailed finite-difference equations.

One of the modifications made in this study of the numerical algorithm is that the pressure and the drag terms are implicitly differenced while the solids stress term is differenced explicitly to save computational time. Implicitly finite-differencing the solids stress term results in more inner loop iterations to meet the convergence criterion. The finite-difference equations are

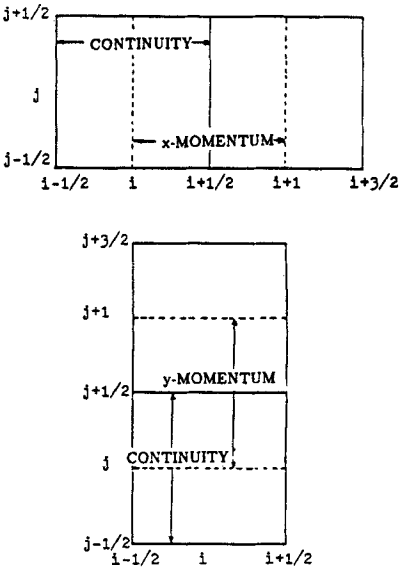

Figure 4. Staggered computational mesh for momentum equations.

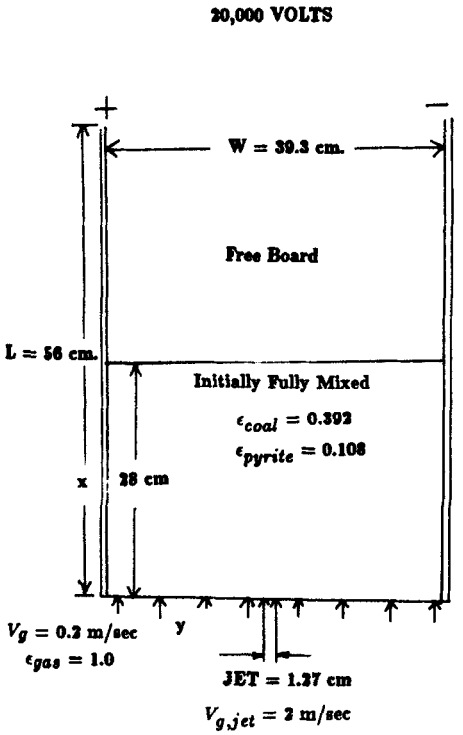

Figure 5. Geometry of system for electrofluidization.

solved by a combination of point relaxation, Newton's, and secant iteration methods for each computational cell, then sweep over the entire bed.

Initial and boundary conditions

The initial and boundary conditions correspond to those for separation of a synthetic mixture of coal and iron pyrites of nearly the same minimum fluidization velocity used in our experiment (Gidaspow et al. 1986a). The fluidized bed described in the reference cited above was 10 cm wide, while the simulation described here is for the larger bed used by Gidaspow et al. (1983a + b), which is now being equipped with electrodes for future experimental studies.

The geometry of the fluidized bed system is shown in Figure 5. The properties of coal and pyrite particles are given in Table 1. The initial solids mixture consisted of fully mixed particles with a 39.2% volume fraction of coal and a 10.8% fraction of pyrite. Gas flowed at a velocity of 7.5 cm/s to keep all the particles in a fluidized state. The pressure distribution was linear. At time zero a central jet was turned on at a velocity of 2 m/s, and the grid flow was increased to 20 cm/s. For the case of electrofluidization, the external power supply of 20,000 V, equivalent to the field strength of 500 V/cm, was also turned on at time zero.

The boundary conditions were as given below; see Figure 5.

Table 1. Properties of Coal and Pyrite Particles

	d_p μm	ρ_p g/cm³	Est. U_{mf} cm/s
Coal	250	1.27	5.1
Pyrite	150	4.6	6.6

B.C.1. At $y = 0^-$ (below the distributor plate, where $0^- = -\Delta y/2$ in program manual, Syamlal, 1985), $\epsilon_l = 1.0$ and $V_l\rho_l$ = constants, as in Figure 5
B.C. 2: At $y = L$, P = atmospheric
B.C. 3: At $x = 0$, $U_1 = U_2 = U_3 = 0$
B.C. 4: At $x = W$, $U_1 = U_2 = U_3 = 0$

The boundary conditions indicate that a specified constant mass of gas flows through the central jet and the distributor grid region, that the bed is open to the atmosphere, and that normal velocities are zero at both walls. Friction with the front and back of the walls is not included in the differential equations or the boundary conditions.

Results of Simulations

Computer simulations were carried out for 1 s of real fluidization time. This permits the passage of three to four bubbles through the bed. Coal and pyrite were initially fully mixed. Two runs were made, one with the external electric field turned on, the other with the field off. The intent was to study and compare the segregation of pyrites from coal and other fluidization characteristics, such as the bubble behavior that causes much of the mixing in electrofluidized and regular fluidized beds.

The computed volume fraction data of coal and pyrite phases were converted into a series of density plots. In the figures, the number of black dots is proportional to the volume fraction of each phase. Figures 6a–f and 7a–f show the density plots for the volume fractions of coal particles with no electric field applied. Figures 8a–f and 9a–f are the corresponding volume fractions of pyrite particles. For the case of electrofluidization, the volume fractions of coal are shown in Figures 10a–f and 11a-f, and those of pyrites in Figures 12a-f and 13a-f.

Typical bubbling phenomena were observed from the concentrations of coal in Figures 6 and 7. Four bubbles were observed during the first second of fluidization. The first bubble formed, propagated, split, and burst. These phenomena were experimentally observed by Seo and by Gidaspow et al. (1985). The second bubble is relatively small and is of cylindrical shape. Bubble splitting and bursting occurred almost simultaneously at a time

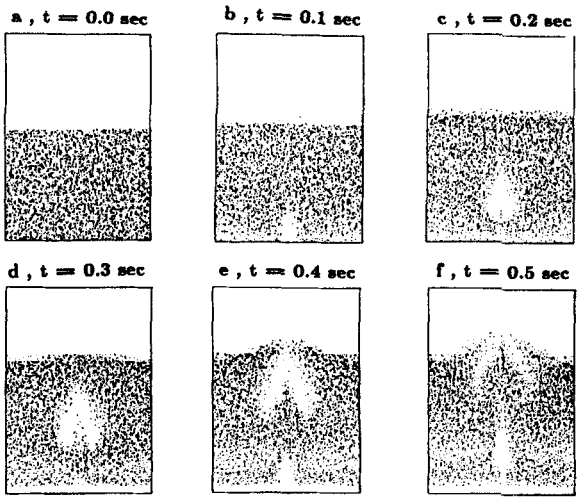

Figure 6. Volume fractions of coal particles with no applied electric field.

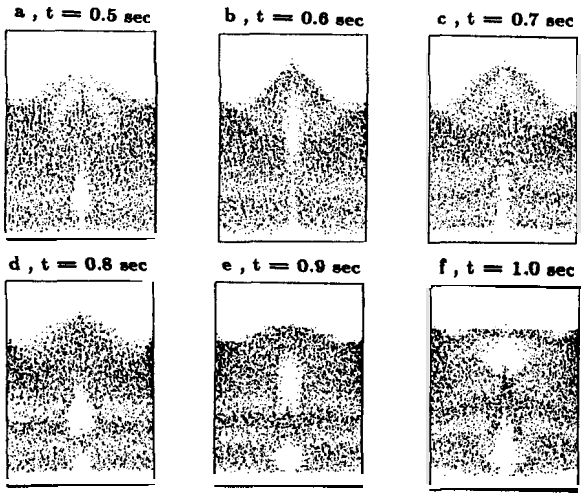

Figure 7. Volume fractions of coal particles with no applied electric field.

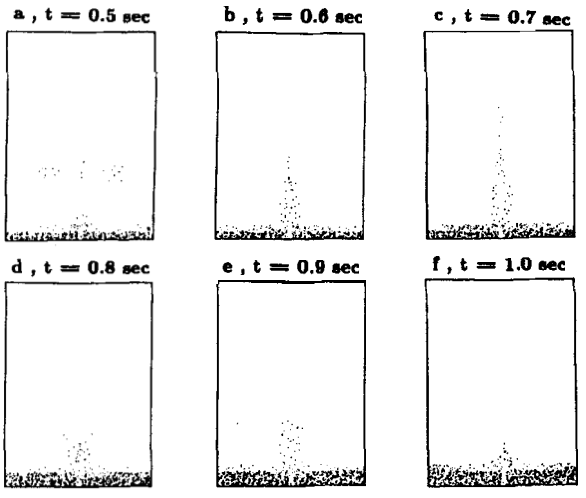

Figure 9. Volume fractions of pyrite particles with no applied electric field.

of 0.7 s. The third bubble formed was of a cylindrical shape that turned into a spherical shape with an obvious drift formation at a time of 1 s. The fourth bubble formed was spherical; however, at the end of the simulation it had a tendency to coalesce with the third bubble. Wake formation was also visible for the first three bubbles.

Density plots of pyrite concentrations, Figures 8 and 9, show the segregation of the pyrite from coal. These phenomena are mainly due to the settling of the pyrites. Pyrite is almost four times heavier than coal. In a later part of the simulations, portions of pyrites were carried up by the jet stream. These particles also contribute to the drift formations.

The bubbling phenomena in electrofluidization can be seen from the coal concentrations, Figures 10 and 11. Instead of four, only three bubbles were computed. This is in agreement with the observed lower bubble frequency characteristic of electrofluidized beds (Katz and Sears, 1969; Clover, 1976; Ademoyega, 1981). The bubbles are smaller than those for the case of no applied electric field. The passage of the bubbles is not limited to the centerline. After formation at the bottom, the bubbles first travel toward the positive electrode due to the motion of the negatively charged particles toward the positive electrode.

Since particles tend to move toward the positive electrode, the upper portion of the bed near the negative electrode becomes free of particles. Bubbles then turn their direction toward this low-pressure region at a time of 0.5 s. Eventually, bubbles burst in this part of the bed at times of 0.6 or 0.7 s. This creates a void in the region near the positive electrode. The particles then fall. These phenomena were computed for both the first and the second bubbles. Wave formation at the interface between the freeboard and the bed was also predicted by this model.

Separation of pyrite from the coal in an electrofluidized bed can be seen from the density plots of pyrite concentrations, Figures 12 and 13. Pyrite particles rapidly move toward the positive electrode, leaving a pyrite-free coal near the negative electrode. The pyrite particles are also seen to climb the wall, corresponding to the observed situation (Gidaspow et al. 1986a). In a batch fluidized bed the pyrites stick to the electrode. This sticking of

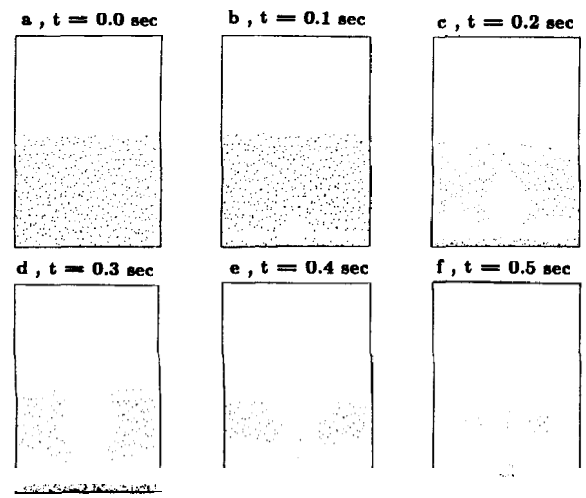

Figure 8. Volume fractions of pyrite particles with no applied electric field.

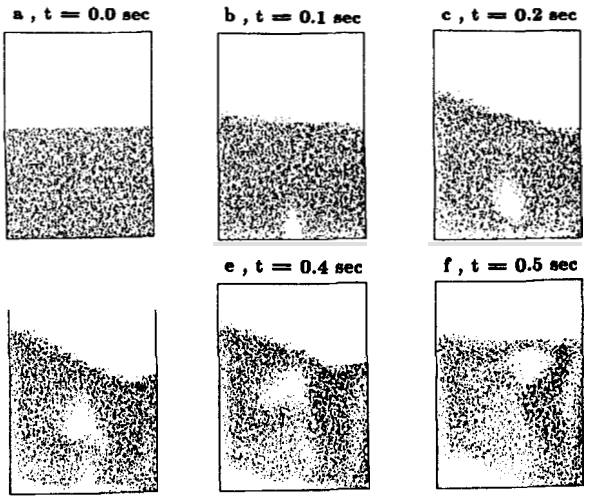

Figure 10. Volume fraction of coal particles with 500 V/cm electric field strength.

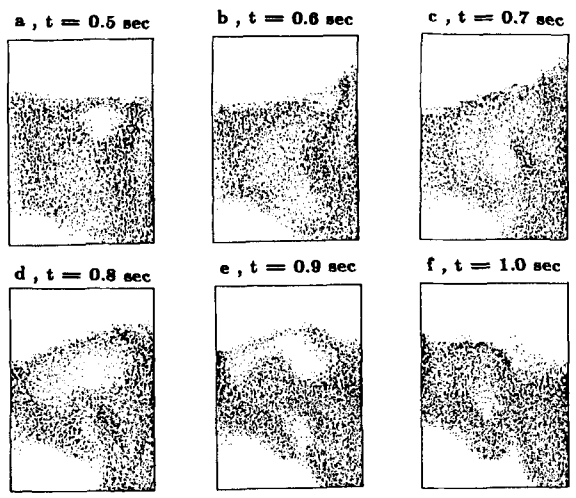

Figure 11. Volume fractions of coal particles with 500 V/cm electric field strength.

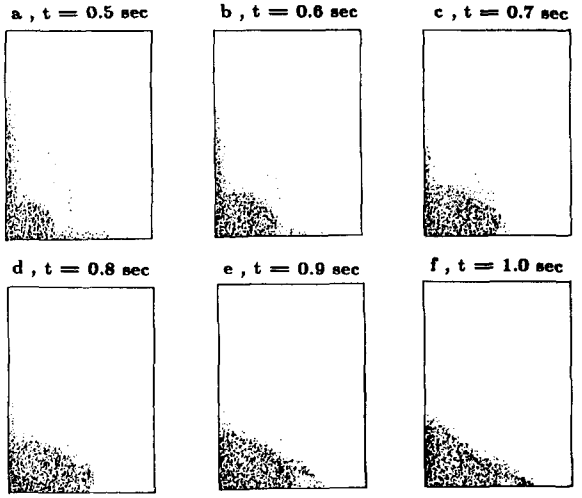

Figure 13. Volume fractions of pyrite particles with 500 V/cm electric field strength.

the particles to the electrode was solved by withdrawing the pyrites through sieve type electrodes.

Electrophoretic mobility of pyrites

From the computed pyrite concentration profiles as a function of time, we can estimate the electrophoretic mobility of the pyrite particles. This electrophoretic mobility is needed for a rational design of a continuous electrofluidized bed. To obtain a clean coal stream in a continuous bed we require that $V_{pyrite} \geq V_{coal}$ through the sieve electrode, where V is the velocity. The pyrite velocity is related to the electrophoretic mobility by means of the relation

$$V = EM \cdot E \tag{20}$$

where EM is the electrophoretic mobility and E is the applied electric field. Hence, knowledge of EM will permit us to obtain an optimum withdrawal rate of the coal in our continuous (Gidaspow et al., 1986a) electrofluidized bed.

Figure 14 shows the computed 2% contours of pyrite concentrations as a function of operating time. The electrophoretic mobility of the pyrite particles in this electrofluidized bed can be estimated by locating a pyrite-free 2% interface at various times. The locations of the interfaces and the estimated electrophoretic mobilities are shown in Table 2.

It is noted here that the locations of the pyrite-free interfaces are determined at 14 cm above the distributor. They are the distances away from the negative electrode. Electrophoretic mobilities are calculated for each time interval of the operation. Higher electrophoretic mobilities were obtained during 0.3–0.4

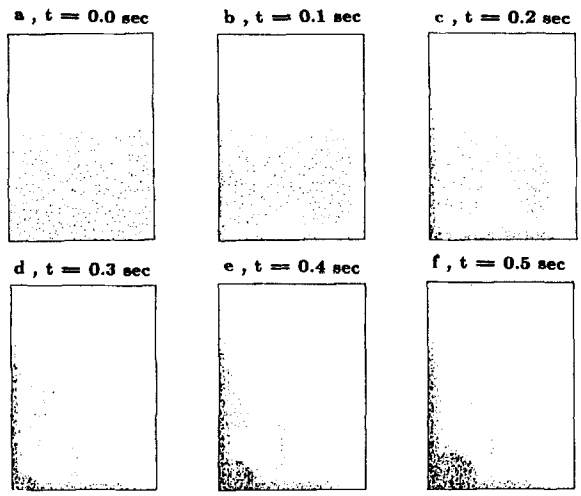

Figure 12. Volume fractions of pyrite particles with 500 V/cm electric field strength.

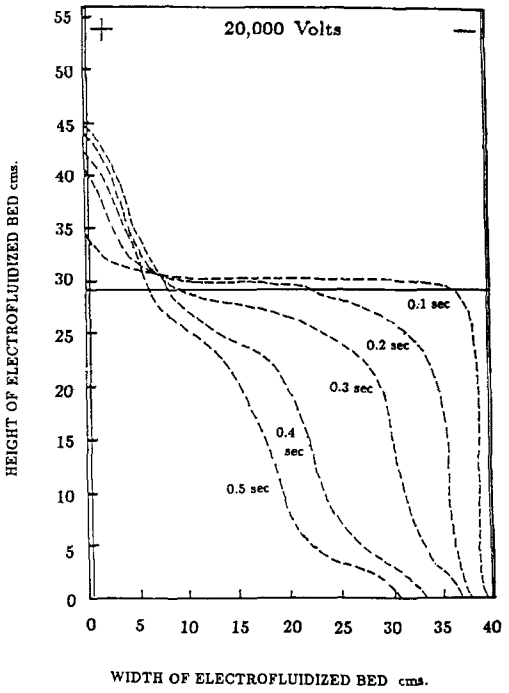

Figure 14. Horizontal components of pyrite velocities at various times in electrofluidized bed.

Table 2. Computed Electrophoretic Mobility of Pyrite Particles

Time s	Locations of Pyrite-free Interfaces cm	Est. *EM* (cm/s)/(V/cm)
0.0	0.0	—
0.1	1.14	0.023
0.2	3.81	0.053
0.3	9.52	0.114
0.4	17.1	0.152
0.5	22.1	0.099

s of operation time. This could be the result of the bubbling in the fluidized bed. Pyrite particles are passing through the bubbles with higher velocities. The average electrophoretic mobility of pyrites for 0.5 s of fluidization is 0.088 (cm/s)/(V/cm). This mobility is equivalent to 44 cm/s or about 14% of the Stokes terminal velocity.

The horizontal components of pyrite velocities across the fluidized bed at 8, 16, 24, and 32 cm above the distributor at various operating times are presented by Shih (1986). Figure 15 shows typical results. At 0.1 s of fluidization, the pyrites are moving at an average velocity about 35 cm/s toward the positive electrode. The velocities fluctuate, but remain in the range of 30 to 60 cm/s.

Shapes and sizes of bubbles

The correct prediction of bubbles in fluidized beds is one of the key issues. Bubbles cause much of the mixing and segregation. The bubbles in electrofluidized bed are generally smaller and tend to be of a more elliptical shape than those in regular fluidized beds. The computed bubble sizes are compared in Table 3 for the two kinds of beds. A bubble is interpreted to be a region of void greater than 0.8.

The size of each bubble listed in Table 3 is the largest size computed during 1 s of fluidization. Many researchers have studied bubble sizes in a fluidized bed. Gidaspow et al. (1983b) have reviewed the literature correlations. They modified the correlations for leakage to be applied for the bed used for computations. The modified correlations are as follows:

J. Werther (1976)

$$D_b = D_{b0} + 0.853[1 + 0.0684(h - L_p)] \tag{21}$$

Kato and Wen (1969)

$$D_b = D_{b0} + 1.4\rho_p d_p (h - L_p) \tag{22}$$

where D_{b0} is the initial bubble size, h is the distance above distributor, and L_p is the jet penetration depth. The sizes of the first computed bubble in both the electrofluidized bed and the regular fluidized bed are compared in Table 4 with the predictions of Eqs. 21 and 22.

The bubble sizes predicted by the hydrodynamic model compare very well with the correlations. It is to be noted that the jet penetration depth L_p estimated from Zenz (1968) is negligible compared to h, therefore, L_p was not used in the calculations.

Bed expansion

In most fluidization systems the bed expands when the gas velocity is increased above the minimum fluidization velocity. The expansion is related to the particle characteristics, void, gas velocity, and bubbling phenomena. Table 5 shows the comparison of bed expansions at various operating times for the two computer simulations.

In electrofluidization, faster bed expansion was computed because the bubble size was smaller. The interface between the freeboard and the bed is of a wave shape with fluctuations when the electric field is on. In such case, an average bed height was listed.

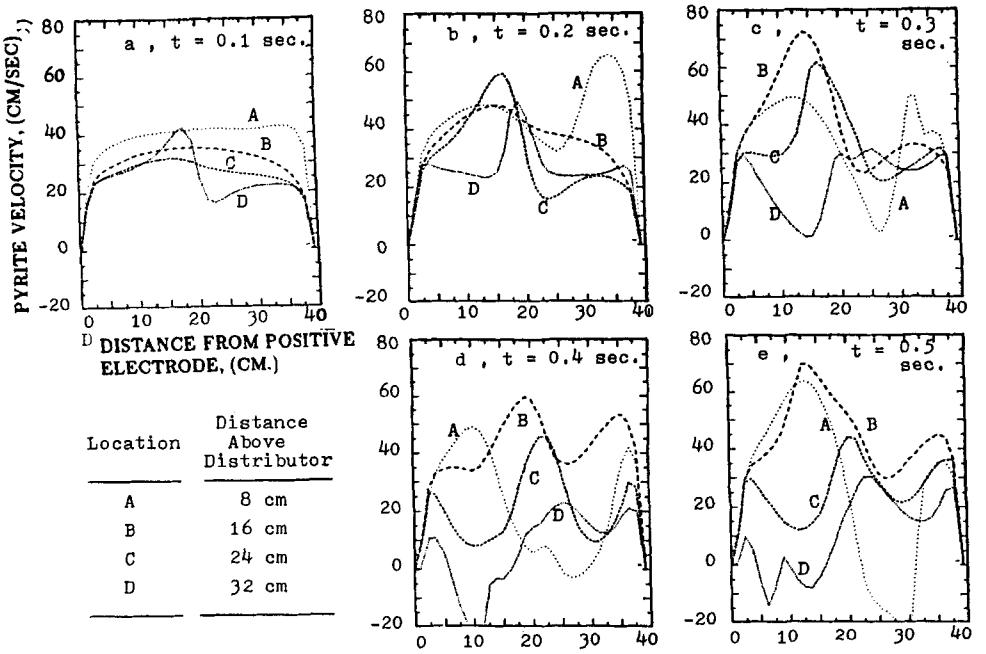

Figure 15. Pyrite-free 2% fronts at various times in electrofluidized beds.

Table 3. Bubble Sizes

	Bubble			
	1st	2nd	3rd	4th
	Without Elec. Field			
Height	11.4	15.1	10.4	13.6
Width	14.1	5.1	11.8	8.6
	With Elec. Field			
Height	8.3	11.3	5.3	—
Width	11.0	8.6	4.3	—

Bubble rise velocities

Among the important properties related to bubbles in fluidized beds is the bubble rise velocity. Many authors have measured the bubble rise velocity in both two- and three-dimensional fluidized beds. Almost all authors (Davidson and Harrison, 1963; Potter, 1971; Rowe, 1971; Leva and Wen, 1971; and others) have summarized their experimental observations or theoretical analyses in a form similar to the equation of Davies and Taylor (1950). In the bubbling region of three-dimensional bed, it is as follows:

$$U_b = 0.71 g^{1/2} D_b^{1/2} \tag{23}$$

where g is the gravitational acceleration and D_b is mean bubble diameter.

Two-dimensional effects on the bubble rise velocities were studied to Pyle and Harrison (1967) and Littman and Homolka (1970). Their results can be summarized by the following equation.

$$U_b = 0.53 g^{1/2} a_b^{1/2} \tag{24}$$

where a_b is the mean radius of the bubbles. Dietz and Melcher (1978) have indicated that an application of an electric field across a fluidized bed results in elimination and deformation of bubbles. Ademoyega (1981) used a high-speed movie camera to measure bubble velocities in an electrofluidized bed of 200 μm silica gel with a central jet at various flow rates and electric field strengths. He found that bubble velocities slowed by about 20% with an electric field strength of 500 V/cm. We have computed our rise velocities and show the results for each bubble in Table 6. The average bubble rise velocity in the electrofluidized bed is about 5 to 25% slower than that in a regular fluidized bed, Table 7.

U_b values calculated from Eqs. 23 and 24 are based on the largest bubble width computed. The predictions from the hydrodynamic model are closer to the three-dimensional correlation, Eq. 23, than to the two-dimensional correlation, Eq. 24. This is because the hydrodynamic model, although two-dimensional, does not include the wall interactions with the face and back walls, and the drag laws used in the computations are basically derived from three-dimensional experiments.

Table 4. Bubble Sizes Predicted by Hydrodynamic Model and Literature Correlations

	Dist. Above Distrib. cm	Hydrody. Model cm	Eq. 21 cm	Eq. 22 cm
Without elec. field	40.1	14.1	12.6	13.3
With elec. field	38.4	11.0	10.9	11.5

Table 5. Bed Expansions

	Time, s				
	0.2	0.4	0.6	0.8	1.0
Without elec. field	1.40	1.59	1.59	1.61	1.53
With elec. field	1.26	1.54	1.59	1.61	1.55

Flow patterns

Figures 16a–e and 17a–e show the gas velocity vector plots at various times. The typical slow bubble profile, in which the gas takes a shortcut through the bubble, can be seen in both the electrofluidized and regular fluidized beds. Due to the movements of the particles toward the positive electrode, some areas in the electrofluidized bed, such as at the top right corner, have a high voidages. The gas also takes advantage of these passages.

Figures 18a–e show the velocity vector plots for coal particles in the electrofluidized bed at various times. Coal particles, although dragged by the pyrites toward the positive electrode in the top left portion of the bed, are circulated back to the negative electrode through the top right corner of the bed. Coal particles in other areas move in a pattern that passes through the bubble at high velocities, and when leaving the bubble they move toward the negative electrode, Figures 18d, e. This process enables us to obtain coal near the negative electrode with no applied electric field. The velocity vector plots for the coal particles are shown in Figures 19a–e. The coal particles were first expelled away from the jet, then when the bubble formed the coal particles were sucked into the bubble. Circulation of coal in the bubble and the formation of a wake are shown in Figure 19c.

Figures 20a–e show the velocity vector plots for pyrites at various instants in the electrofluidized bed. Pyrites are moving toward the positive electrodes with higher velocities when they encounter the bubbles. Some circulation occurred at the top and near bottom of the bed. Some pyrites near the negative electrode settled and then were picked up by the jet. Velocity vector plots for pyrites in the regular fluidized bed are shown in Figures 21a–e. The pyrites moved in a similar pattern to the coal par-

Table 6. Estimations of Bubble Rise Velocities, cm/s

	Bubble			
	1st	2nd	3rd	4th
Without elec. field	98.3	90.8	83.3	60.5
With elec. field	73.8	77.5	79.5	—
Difference, %	25	15	5	—

Table 7. Bubble Rising Velocities, cm/s

	Hydrody. Model	Eq. 23	Eq. 24
Without elec. field	83.2	83.5	44.1
With elec. field	76.9	73.7	39.0

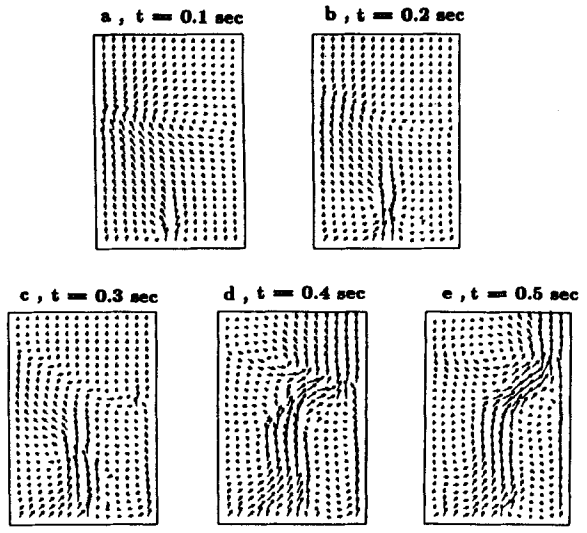

Figure 16. Gas velocities at various times in electrofluidized bed.

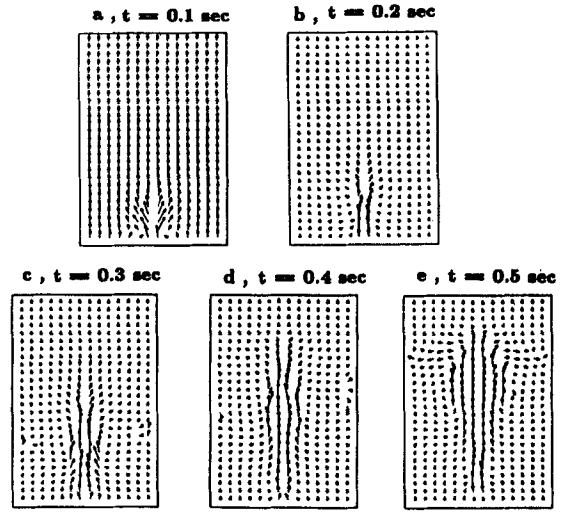

Figure 17. Gas velocities at various times in fluidized bed with no applied electric field.

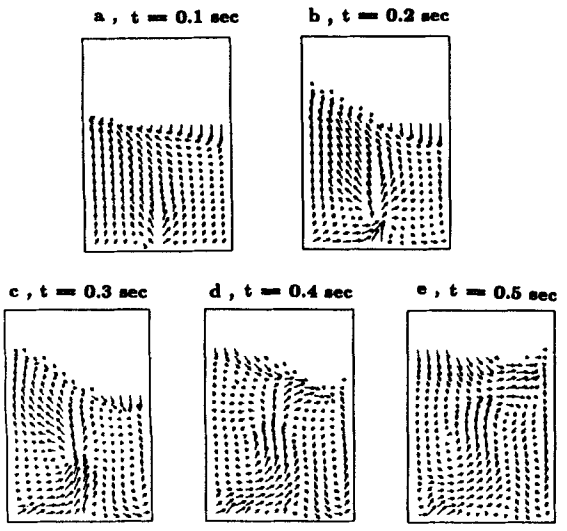

Figure 18. Coal velocities at various times in electrofluidized bed.

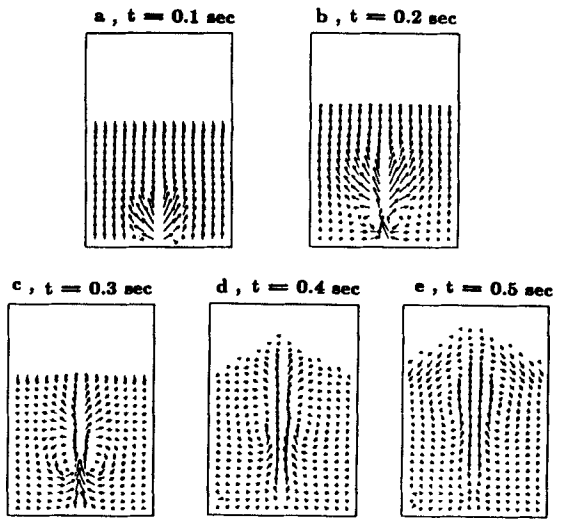

Figure 19. Coal velocities at various times in fluidized bed with no applied electric field.

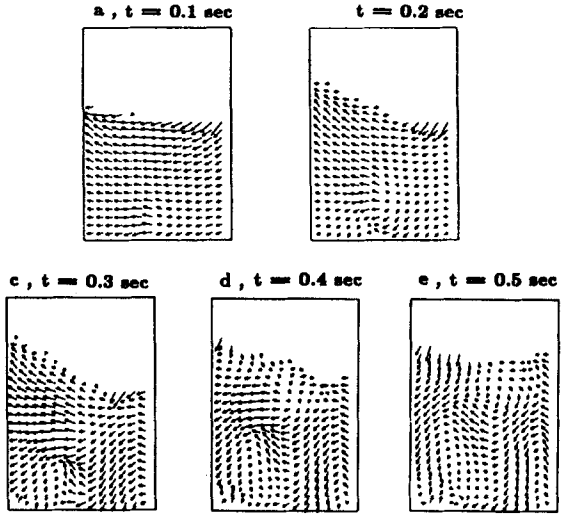

Figure 20. Pyrite velocities at various times in electrofluidized bed.

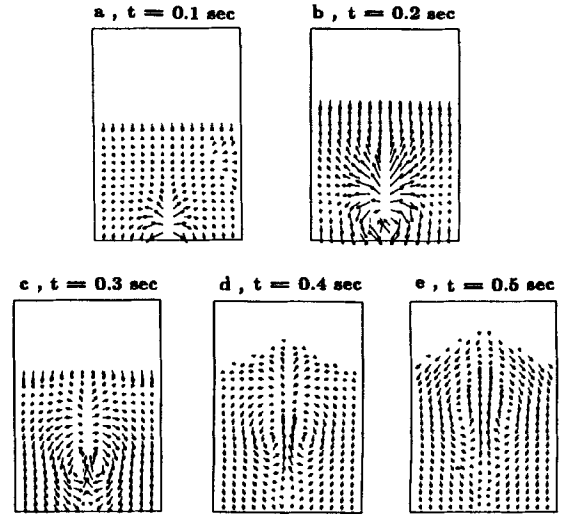

Figure 21. Pyrite velocities at various times in fluidized bed with no applied electric field.

ticles. Circulation of pyrites in the bubble and the formation of a wake are also shown in Figure 21. Since the pyrites are heavier than coal, settling of pyrites can be seen near the bottom of the bed.

Acknowledgment

This study was supported by grants from the Department of Energy and Natural Resources of the State of Illinois and the Coal Research Board, and by the National Science Foundation.

Notation

a_b = bubble radius
a_p = particle radius
C_{Dk} = gas particulate phase k drag coefficient
D_b = bubble diameter
D_{b0} = initial diameter of bubble
d_k = characteristic diameter of particulate phase k
d_p = particle diameter
e = coefficient of restitution
E = externally applied electric field strength
EM = electrophoretic mobility
F_e = electrical force acting on particles
F_g = gravitational force acting on particles
f = function, Eq. 6
G = solid stress modulus
g = gravitational acceleration
h = distance above distributor
K_{kl} = generalized drag coefficient between phases k and 1
L = height of fluidized bed
L_p = jet penetration depth
N = total number of phases
P = system pressure
q = surface charge of particles per unit volume of mixture
Re = Reynolds number for particulate phases
T = system temperature
t = time
U = horizontal component of velocities
U_b = bubble rising velocity
U_{mf} = minimum fluidization velocity
v = velocity vector of phases
V = vertical component of velocities
$V_{s,\text{crit}}$ = critical flow velocity
W = width of fluidized bed

Greek letters

α = non-head-on collision factor, Eq. 9
δ_x, δ_y = mesh sizes
ϵ = volume fraction
μ = viscosity
ϕ = characteristic shape factor of solids phase
ρ = density

Subscripts

k = phase k
1 = gas phase
s = particulate phase

Literature cited

Abel, W. T., M. Zulkoski, G. A. Brady, and J. W. Eckerd, "Removing Pyrite from Coal by Dry Separation Method," U.S. Bureau of Mines, Rept. 7732 (1973).

Ademoyega, B. O., "Characteristics and Conversion in a Catalytic Electrofluidized Bed Reactor," M.S. Thesis, Illinois Inst. Technol., Chicago (1981).

Arastoopour, H., D. Lin, and D. Gidaspow, "Hydrodynamic Analysis of Pneumatic Transport of a Mixture of Two Particle Sizes," *Multiphase Transport*, Hemisphere, Washington, DC, **4**, 1853 (1980).

Arastoopour, H., S. C. Lin, and S. Weil, "Analysis of Vertical Pneumatic Conveying of Solids Using Multiphase Flow Models," *AIChE J.*, **28**, 467 (1982).

Bagnold, R. A., "Experiments on a Gravity-Free Dispersion of Solid Spheres in a Newtonian Fluid Under Shear," *Proc. Roy. Soc.*, **A225**, 49 (1954).

Chiba, S., T. Chiba, A. W. Nienow, and H. Kobayoshi, "Minimum Fluidization Velocity, Bed Expansion, and Pressure-Drop Profile of Binary Particle Mixtures," *Powder Tech.*, **22**, 255 (1979).

Colver, G. M., "Bubble Control in Gas-Fluidized Beds with Applied Electric Fields," ASME-AIChE Heat Transfer Conf., St. Louis (1976).

———, "The Influence of Electric and Magnetic Fields on Air-Fluidized Beds," *Proc. NSF Workshop Fluidization Fluid-Particle Sys. Research Needs Priorities*, 57 (1979).

Davidson, J. F., and D. Harrison, *Fluidized Particles*, Cambridge Univ. Press, (1963).

Davies, R. M., and G. Taylor, "The Mechanics of Large Bubbles Rising Through Extended Liquids and Through Liquids in Tubes," *Proc. Roy. Soc.*, **200A**, 375 (1950).

Dietz, P. W., and J. R. Melcher, "Interparticle Electrical Forces in Packed and Fluidized Beds," *Ind. Eng. Chem. Fundam.*, **17**, 28 (1978).

Ettehadieh, B., "Hydrodynamic Analysis of Gas-Solid Fluidized Beds," Ph.D. Diss. Illinois Inst. Technol. (1982).

Fedors, R. F., and R. F. Landel, "An Empirical Method of Estimating the Void Fraction in Mixtures of Uniform Particles of Different Size," *Powder Tech.*, **23**, 225 (1979).

Gidaspow, D., "Hydrodynamics of Fluidization and Heat Transfer: Supercomputer Modeling," *Appl. Mech. Rev.*, **39**(1), 1 (1986).

Gidaspow, D., and B. Ettehadieh, "Fluidization in Two-Dimensional Beds with a Jet. 2: Hydrodynamic Modeling," *Ind. Eng. Chem. Fundam.*, **22**, 193 (1983a).

Gidaspow, D., Y. C. Seo, and B. Ettehadieh, "Hydrodynamics of Fluidization: Experimental and Theoretical Bubble Sizes in a Two-Dimensional Bed with a Jet," *Chem. Eng. Commun.*, **22**, 253 (1983b).

Gidaspow, D., and M. Syamlal, "Solid-Gas Critical Flow," Paper No. 73e, microfiche preprint, AIChE Ann. Meet. Chicago (Nov., 1985).

Gidaspow, D., M. Syamlal, and Y. Seo, "Hydrodynamics of Fluidization: Supercomputer Generated vs. Experimental Bubbles," to be published in *J. Powder Bulk Solids Technol.* (1987).

Gidaspow, D., D. T. Wasan, S. Saxena, Y. T. Shih, R. P. Gupta, and A. Mukherjee, "Electrostatic Desulfurization of Coal in Fluidized Beds and Conveyors," microfiche preprint, AIChE Ann. Meet. Miami Beach (Nov. 1986a).

Gidaspow, D., M. Syamlal, and Y. Seo, "Hydrodynamics of Fluidization of Single and Binary Size Particles: Supercomputer Modeling," *Proc. 5th Eng. Found. Conf. Fluidization*, Elsinore, Denmark, 1 (1986b).

Gwyn, J. E., "Interactive Forces in Contraflow Ball/Particulate Fluidized Beds," *Proc. 5th Eng. Found. Conf.* Fluidization, Elsinore, Denmark, 321 (1986).

Inculet, I. I., M. A. Bergougnou, and J. D. Brown, "Electrostatic Beneficiation of Coal," *Physical Cleaning of Coal*, Y. A. Liu, ed., Dekker, 87 (1982).

Jackson, R., "The Mechanics of Fluidized Beds," *Trans. Inst. Chem. Eng.*, **41**, 13 (1963).

Johnson, T. W., and J. R. Melcher, "Electromechanics of Electrofluidized Beds," *Ind. Eng. Chem. Fundam.*, **14**, 146 (1975).

Kato, K., and C. Y. Wen, "Bubble Assemblage Model for Fluidized-Bed Catalytic Reactors," *Chem. Eng. Sci.*, **24**, 351 (1969).

Katz, H., U.S. Patent 3,304,249 (1967).

Katz, H., and J. T. Sears, "Electric Field Phenomena in Fluidized and Fixed Beds," *Can. J. Chem. Eng.*, **47**, 50 (1969).

Kunii, D., and O. Levenspiel, *Fluidization Engineering*, Wiley, New York (1969).

Leva, M., and C. Y. Wen, *Fluidization*, J. F. Davidson and D. Harrison, eds., Academic Press, London, Ch. 14 (1971).

Littman, H., and G. A. J. Homolka, "Bubble Rise Velocities in Two-Dimensional Gas-Fluidized Beds from Pressure Measurements," *Chem. Eng. Symp. Ser.*, **105**, 66, 37(1970).

Moore, A. D., *Electrostatics and Its Applications*, Wiley, New York (1973).

Nakamura, K., and C. E. Capes, "Vertical Pneumatic Conveying of Binary Particle Mixtures," *Fluidization Technology*, Keairns, ed., Hemisphere, Washington, DC, 159 (1976).

Piepers, H. W., E. S. E. Cottar, A. H. M. Verkooijen, and K. Rietma, "Effects of Pressure and Type of Gas on Particle-Particle Interaction

and the Consequences for Gas-Solid Fluidization Behaviour," *Powder Tech.*, **37**, 55 (1984).
Pyle, D. L., and D. Harrison, "The Rising Velocity of Bubbles in Two-Dimensional Fluidized Beds," *Chem. Eng. Sci.*, **22**, 531 (1967).
Potter, O. E., *Fluidization*, J. F. Davidson, and D. Harrison, eds., Academic Press, London, Ch. 7 (1971).
Ralston, O. C., *Electrostatic Separation of Mixed Granular Solids*, Elsevier, (1961).
Rietma, K., and S. M. P. Mutsers, "The Effect of Interparticle Forces on Expansion of a Homogeneous Gas-Fluidized Bed," *Proc. Int. Symp.* Fluidization, Toulouse, France, 32 (1973).
Rivard, W. C., and M. D. Torrey, "K-FIX: A Computer Program for Transient, Two-Dimensional, Two-Fluid Flow," LA-NUREG-6623, Los Alamos (1977).
Rosensweig, R. E., M. Zahn, W. K. Lee, and P. S. Hagan, "Theory and Experiments in the Mechanics of Magnetically Stabilized Fluidized Solids," *Theory of Dispersed Multiphase Flow*, Academic Press, 359 (1983).
Rowe, P. N., *Fluidization*, J. F. Davidson and D. Harrison, eds., Academic Press. London, Ch. 4 (1971).
Rowe, P. M. and A. W. Nienow, "Minimum Fluidization Velocities of Multicomponent Particle Mixtures," *Chem. Eng. Sci.*, **30**, 1365 (1975).
Seo, Y., "Fluidization of Single and Binary Size Particles," Ph.D. Diss., Illinois Inst. Technol., Chicago (1985).
Shih, Y. T., "Hydrodynamics of Separation of Particles: Sedimentation and Fluidization," Ph.D. Thesis, Ill. Inst. of Tech., Aug. 1986.
Soo, S. L., *Fluid Dynamics of Multiphase Systems*, Blaisdell, Waltham, MA (1967).
Syamlal, M., "Multiphase Hydrodynamics of Gas-Solids Flow," Ph.D. Diss., Illinois Inst. Technol., Chicago (1985).
Werther, J., "Bubble Growth in Large-Diameter Fluidized Beds," *Fluidized Technology*, I, Hemisphere, Washington, DC, 215 (1976).
Yang, W. C., and D. L. Keairns, "Rate of Particle Separation in a Gas-Fluidized Bed," *Ind. Eng. Chem. Fundam.*, **21**, 228 (1982).
Zahedi, K., and J. R. Melcher, "Electrofluidized Beds in the Filtration of a Submicron Aerosol," *J. Air Pollution Control Asso.*, **26**, 345 (1976).
Zenz, F. A., "Bubble Formation and Grid Design," *Inst. Chem. Eng. Symp. Ser.*, **30**, 136 (1968).

Manuscript received Sept. 9, 1986, and revision received Jan. 22, 1987.